57-Year California Reanalysis Downscaling at 10 km (CaRD10)

-- Part 1. System Detail and Validation with Observations

by

Masao Kanamitsu and Hideki Kanamaru

Scripps Institution of Oceanography

University of California, San Diego

For publication in *Journal of Climate*

Submitted May 7, 2006
Revised November 27, 2006

Corresponding author: Dr. Masao Kanamitsu, Mail Code 0224; CRD/SIO/UCSD; 9500 Gilman Drive; La Jolla, CA 92093-0224
E-mail: mkanamitsu@ucsd.edu

Abstract

For the purpose of producing datasets for regional scale climate change research and application, the NCEP/NCAR Reanalysis for the period 1948-2005 was dynamically downscaled to hourly, 10 km resolution over California using the Regional Spectral Model.

This is a Part 1 of two part paper, describing the details of the downscaling system and comparing the downscaled analysis (CaRD10) against observation and global analysis. An extensive validation of the downscaled analysis was performed using station observations, Higgins gridded precipitation analysis and Precipitation-elevation Regression on Independent Slopes Model precipitation analysis.

In general, the CaRD10 near-surface wind and temperature fit better with regional scale station observations than the NCEP/NCAR reanalysis used to force the regional model, supporting the premise that the regional downscaling is a viable method to attain regional detail from large scale analysis. This advantage of CaRD10 was found on all time scales, ranging from hourly to decadal scales, i.e. from diurnal variation to multi-decadal trend.

Dynamically downscaled analysis provides ways to study various regional climate phenomena of different time scales because all produced variables are dynamically, physically and hydrologically consistent. However, the CaRD10 is not free from problems. It suffers from positive bias in precipitation for heavy precipitation events. The CaRD10 is inaccurate near the lateral boundary where regional detail is damped by the lateral boundary relaxation. It is important to understand these limitations before the downscaled analysis is used for research.

1. Introduction

Climate research, particularly application studies for water, agriculture, forestry, fishery and energy management require fine scale multi-decadal information of meteorological, oceanographic and land states. Unfortunately, spatially and temporally homogeneous multi-decadal observations of these variables in high horizontal resolution are non-existent. Some long term surface records of temperature and precipitation exist, but the number of observations is very limited and the measurements are often contaminated by changes in instrumentation over time. Some climatologically important variables, such as soil moisture, surface evaporation, and radiation are not even measured on most of the continental U.S.

Reanalysis is one approach to obtaining long term homogeneous analysis of needed variables. Unfortunately, the horizontal resolution of global reanalysis is of the order of 100 to 200 km, too coarse for many application studies. Recently, regional reanalysis over North America was conducted (North American Regional Reanalysis, (NARR), Mesinger et al, 2006). The horizontal resolution of 32 km and the duration of 25 years used in that study are still not completely satisfactory for application requirements, but the product is definitely valuable. We can expect to see exciting results soon from studies using the NARR.

In this paper, we present another attempt to produce even higher resolution regional "reanalysis" over a longer period for the state of California using a dynamical downscaling technique (California Reanalysis Downscaling at 10 km; CaRD10 hereafter). This method is based on the concept that small scale detail can be attained by laterally forcing the high resolution regional model with large scale analysis. The major

assumption made in this process is that the small scale features are purely forced by large scale and the small scale never feeds back to the large scale. This assumption holds well when the large scale forcing is strong (e.g. during winter and transient seasons), but may fail when the forcing is weak (e.g. during summer).

The essential difference between the dynamical downscaling method and data assimilation, which is used in NARR and in all the global reanalyses, is that the former does not utilize station observations to correct model forecast error. In this context, the dynamical downscaling can be referred to as "regional data assimilation without observation" (von Storch et al, 2000). As described later, dynamical downscaling can be improved by forcing the large scale part of the field *within* the regional domain. This process reduces the forecast error of the "large scale" part of the regional model, particularly when the domain is large. With this correction of large scale, the dynamical downscaling can be better termed "regional data assimilation without *regional* scale observation," since the regional model knows the large scale observation indirectly through the global reanalysis.

The major objective of Part 1 of this two-part paper is to demonstrate that the dynamical downscaling is capable of reproducing small scale detail which agrees better with station observations than the coarse resolution analysis, without injecting small scale observation. In other words, the dynamical downscaling can serve as a regionalization of coarse resolution data assimilation analysis without conducting expensive high resolution data assimilation.

In Part 2 we describe a detailed comparison of the downscaled analysis with NARR. In this part of the study, we aim at understanding the role of data assimilation for

small scale analysis and the importance of high horizontal resolution. We also demonstrate the implied uncertainties in regional analyses.

This paper is organized as follows: In section 2, the model and downscaling procedures are discussed. In section 3, validation of the analysis based on station observation is presented. Section 4 compares the CaRD10 precipitation with gridded precipitation analysis, namely Higgins analysis and PRISM (Precipitation-elevation Regression Independent Slopes Model) data, and Section 5 concludes the paper.

2. Model and dynamical downscaling procedure

2.1. The Regional Spectral Model

The Regional Spectral Model (RSM, Juang and Kanamitsu, 1994) is used in this study. The model originates from the one used at the National Centers for Environmental Prediction (NCEP), but the code was updated with greater flexibility and much higher efficiency (Kanamitsu et al., 2005) at the Scripps Institution of Oceanography. The RSM utilizes a spectral method (with sine and cosine series) in two dimensions. A unique aspect of the model is that the spectral decomposition is applied to the difference between the full field and the time-evolving background global analysis field. The model integration procedure mimics the prediction of perturbations, but it is not the perturbation prediction equation that is integrated in time. The procedure would probably be better named as *optimum spectral perturbation filtering method*, in which full field minus base field, both of which are defined within the domain, is used to apply sine and cosine filter.

The model is based on the primitive equation system and it consists of momentum equation, thermodynamic equation, mass conservation equation and moisture equation. The primitive equation system is based on an approximation that the horizontal scale is

much larger than the vertical scale. This approximation places a limit to the use of horizontal resolution depending on the vertical scale of the phenomena. The regional scale phenomena, such as sea breeze, mountain-valley breeze and many of the flow regimes appearing along the coast of California are confined within the marine boundary layer and have the vertical scale of 1-3 km. Therefore, the horizontal grid size of the quasi-hydrostatic equation model can be as small as 5-10 km. On the contrary, the deep convective system which appears in the summertime over the Midwest has a vertical scale of more than 10 km and therefore, a horizontal resolution of 30 km or larger is preferred. For the downscaling performed in this study, a horizontal resolution of approximately 10 km is used. The use of this rather high resolution is based on the dominance of relatively small vertical scale phenomena in California The choice is also based on the more practical desire to resolve complex topography in California as much as possible for the purposes of water management application.

The only difference in the dynamical core used in this study from the original RSM is the application of a process splitting time scheme (Williamson, 2002), in which physical processes are computed in parallel with the dynamical forcing terms, as opposed to computing them in a serial manner. This scheme saves considerable computational time for parallel computing since it reduces the communication between the processors, by as much as a factor of two. Other details of the parallelization and optimization of the model are described in Kanamitsu et al (2005a).

The physical processes included in the model are listed in Table 1. The physical parameterization schemes used in RSM are fully tested in its global model counterpart - the Global Spectral Model - with ensemble AMIP type runs. The skill of the simulation

is reasonable and comparable to many other global models (Robertson et al., 2004). For the application of the schemes to high resolution regional downscaling by RSM, no explicit changes of the physical processes are applied, except the horizontal diffusion.

Among these physical processes, particular mention will be given to the Oregon State University Land Scheme (Pan and Mahrt, 1987) and the radiation. The land scheme consists of two soil layers, 10cm and 190cm thick, where soil moisture and soil temperature are predicted. Evaporation from the land surface is divided into two parts; direct evaporation and transpiration. The formula of Chen and Dudhia (2001a, b) is used for direct evaporation (Kanamitsu and Mo, 2003). The snow model is a simple 1-layer energy balance model. Specifications of the land surface characteristics are described in Section 2.4. Other details of the scheme are described in Chen et al. (1996). The vegetation type, vegetation fraction, and soil type are fixed climatology and do not evolve during the 57 years of downscaling.

Both short and long wave radiation schemes are taken from M.-D. Chou (Chou and Suarez 1994; Chou and Lee 1996). Cloudiness is computed from relative humidity and vertical motion, as well as from marine boundary layer depth and intensity (Slingo, 1987). These clouds interact with the radiation scheme.

As will be mentioned later in section 2.3, area average temperature and moisture in the regional domain are nudged to those of the reanalysis by the scale selective bias correction (SSBC) scheme (Kanamaru and Kanamitsu, 2006) to be described in more detail later. Therefore the effects of CO_2 and aerosol on the downscaled analysis of large scale free atmosphere will be minimal. However, the surface fluxes will certainly be affected by CO_2 and aerosol. These atmospheric compositions impact land states such as

soil moisture and snow through the change in radiation flux reaching the ground. In CaRD10, the CO_2 concentration is fixed at 348 ppm throughout the 57 years of integration. The aerosol is also fixed at seasonal climatological value by Koepke et al. (1997). This is one of several simplifications made in this downscaling and caution needs to be exercised when the downscaled products are used for diagnostics and application.

2.2. Model domain and topography

The model domain is shown in Figure 1. The Mercator projection true at 60N is used in this study. The domain covers the area from 29.466N to 45.719N, and 128.203W to 111.563W. The model surface elevation is also shown in Fig. 1. This domain is selected to focus on the state of California and the neighboring states, but it also incorporates requests from the ocean research community. Note that the major limiting factor of the domain size is computer resource availability. It should also be noted that the lateral boundary nudging zone extends to approximately 20-25 grid points from the boundary, reducing the useable domain. These limitations will be remedied in the simulations with exactly the same downscaling system over the contiguous United States, currently in progress in collaboration with the Earth Simulator Center in Japan.

2.3. Scale Selective Bias Correction (SSBC)

The accuracy of the dynamically downscaled analysis depends on two factors: the assumption of one-way interaction and the accuracy of the regional model itself. The former is a fundamental assumption in dynamical downscaling, which sets the theoretical limit to the methodology. The latter factor consists of inaccuracies due to numerics (accuracy of the discretization method, and the treatment of the time evolving lateral

boundary conditions) and inaccuracies of the physical processes. These inaccuracies can be reduced in principle by improving each component, but this requires diligent and continuous efforts, as seen from the fact that many operational numerical forecast centers are spending most of their resources on this sole purpose.

Kanamaru and Kanamitsu (2006) showed that the growth of *large scale error* spanning the regional domain has been the major cause of inaccuracies in the dynamical downscaling procedure using RSM, and the SSBC scheme can reduce this error. The scheme consists of three components: 1) nudging of the large scale part of the wind perturbation towards zero, 2) removing the area average perturbation of temperature and moisture at every model level and 3) adjusting the area mean perturbation logarithm of surface pressure to the corresponding difference of logarithm of surface pressure due to the area mean difference in the global and regional topography. The combination of these procedures reduces the large scale error and improves the simulation of precipitation, makes the downscaling insensitive to the model domain, and allows the use of much weaker lateral boundary relaxation in RSM. We apply this method to reduce the error greater than 1000 km. This cutoff scale is based on the average distance of radiosonde observations in the U. S. (approximately 250 km; Archer and Jacobson, 2003), and the resolution of the NCEP-NCAR reanalysis, which is about 200 km. In CaRD10, however, SSBC is mostly effective on the area average and the largest scale because the domain is about the size of 1000 km x 1600 km.

2.4. Lateral forcing, SST and land characteristics

The lateral forcing is taken from NCEP-NCAR global reanalysis, hereafter referred to as NNR (Kalnay et al., 1996), which is the only reanalysis that goes back to the late 1940's. The 200 km resolution global Reanalysis is directly downscaled to 10 km in this study. This large downscaling ratio by RSM, about 20, did not cause any appreciable problem in the regional domain away from the lateral boundary relaxation zones, as envisaged by Juang and Hong (2001). The 6-hourly reanalysis at model sigma levels is used to force the regional model. The RSM model levels are chosen to match the reanalysis model levels, such that vertical interpolation is avoided. The tendency of the global field is assumed to be constant during the 6 hours.

The ECMWF 40-year Reanalysis Sea Surface Temperature is used in the downscaling. This SST (Fiorino 2004) is a combination of the SST analyses from the Hadley Center, the United Kingdom Met Office (monthly mean HadISST, prior to and including 1981) and NCEP (weekly NCEP 2DVAR SST, after 1982 inclusive), cleaned up at the ice edges and interpolated to daily analysis using the mean conserving interpolation scheme (Taylor et al, 2000). We selected this SST primarily because it has been thoroughly checked through use in several reanalyses, and the data were readily available.

Land characteristics, namely vegetation types, vegetation fraction, and soil types are taken from the United States Geological Survey (USGS) compilation. The original 10-min resolution data were re-sampled to 30-min resolution to reduce the data volume size, and were then utilized in the downscaling. The Oregon State University Land Model used in this study recognizes 12 types of vegetation as well as 16 types of soil.

For the vegetation fraction, seasonally varying climatology is used (thus, no long-term change in land characteristics is incorporated).

Soil moisture and soil temperature are predicted by the model during the nesting period of 6 hours. These predicted values are carried to the next nesting period, thus they evolve with time during the entire period of downscaling and interact with near surface atmosphere. No attempt to prevent the land state from drifting to its own climatology was made. As shown later, no apparent drift was observed during the 57 years of downscaling.

The topography is taken from USGS GTOPO30 and interpolated directly to the model grid. The variance of topography used in the gravity wave drag parameterization (Alpert et al 1988) is computed as a variance of 30-minute topography within the regional model grid of 10 km.

2.5. Integration procedure

The downscaling is performed in three streams: 1948-69, 1968-89 and 1988-2005. The initial condition of the atmosphere and land is taken from the global reanalysis at 00UTC on January 1, 1948, linearly interpolated to regional model grid. In order to avoid spin-up of soil moisture, the three streams overlap over two-year periods, 1968-69 and 1988-89. The discontinuity in soil moisture after the two year overlap becomes very small.

3. Validation of the downscaled analysis against station observations

We demonstrate that the downscaled analysis fits better with observation than the coarse resolution global analysis, particularly with near surface observation in a regional scale. Since the accuracy of the downscaled analysis is expected to vary with the time

scale, we performed the validation against surface observations by separating the time scale to hourly, daily, monthly, and decadal, including long term trend. The station observation locations used for validation are plotted in Fig. 1 and listed in Table 2. There are three types of station observations. Fifteen hourly buoy observations (courtesy of Steve Taylor; station names start with "b"), stations from the United States Historical Climatology Network (USHCN) (http://cdiac.ornl.gov/epubs/ndp/ushcn/newushcn.html) for monthly and daily means (three coast locations, "c", six valley locations, "v", and two mountain locations, "m"), and 12 daily airport station observations from the National Climatic Data Center (NCDC; three letter abbreviations).

3.1 Daily Scale

3.1.1 Wind over coastal ocean

The normalized wind vector anomaly correlation (Breaker et al, 1994) and vector root mean square error (RMSE) of two daily analyses, CaRD10 and NNR against fifteen buoy observations (Table 2.a and Fig.1) during January and August, 2000 are computed (Table 3). This validation is of particular interest since the effect of local geography on coastal ocean wind is probably much simpler than that over land. The locations of the buoys used in this comparison are shown as station names starting with 'b' in Fig. 1. The statistical significance test performed separately for u- and v-components showed that the vector correlation lower than approximately 0.61 may occur by chance at a 95 % confidence level. Table 3 clearly shows that for almost all the stations, CaRD10 has higher correlation and lower RMSE than NNR in January. The statistical significance shows that the CaRD10 correlation is better than NNR only at a few stations (b14, b25, b26, and b42) but systematic improvements in many other stations suggest that the

superiority of CaRD10 over NNR is real. The improvement is very large for buoy b25, which is located to the south of Point Conception, an area characterized by weaker winds with more temporal and spatial variability. This location is also known as the place where the Catalina Eddy forms (more detail in section 3.3 and Part 2), The average vector correlation and RMSE for all the buoys compared here are shown in the bottom row of Table 3. Compared to NNR, the improvement of the RMSE in the downscaling is impressive. As we discuss in section 3.4, caution should be exercised when simply comparing the area averaged skills, due to the difference in spatial sampling between coarse and fine resolution analyses.

3.1.2 Wind over land

We performed similar comparisons on wind over land using 12 airport stations (Table 4). The station locations are shown as red cross-hair marks in Fig. 1 and listed in Table 2.c. Overall, the fit of the two analyses to the land stations are much worse than those over ocean. This is expected since the more complex surface topography on land produces a stronger influence on winds. The differences in fit between the two analyses are more diverse, but CaRD10 seems to be consistently better than NNR, both in terms of correlation and RMSE. The average correlation and RMSE for all the stations are shown in the bottom row of Table 4. The CaRD10 fits better due to the detailed 10 km resolution topography.

3.1.3 Near-surface temperature over land

Table 5 compares the average of correlation, RMSE, and bias of daily mean and max/min temperature at 12 land stations in California for January and August, 2000 (same stations as the wind verification over land). The CaRD10 correlation ranges from

0.5 to over 0.9 for individual stations (not shown). For the daily mean temperature, the CaRD10 result is about the same as NNR during January, and better in August. In terms of mean bias removed RMSE, the CaRD10 is better in January and about the same in August.

For max/min temperature, the CaRD10 correlation is higher than that of NNR, with the exception of daily minimum temperature in January, and the RMSE of CaRD10 is less than that of NNR with the exception of daily max temperature in August. Overall, the improvement of CaRD10 over NNR is not very large. When looking at individual stations, the correlations and RMSE of daily max/min temperature with observations are mixed However, there is no station where CaRD10 fails to outperform NNR both in max and min temperatures (not shown).

For the station elevation corrected mean bias, the CaRD10 has a smaller bias than NNR in daily mean and maximum temperatures possibly due to the superior representation of surface characteristics in CaRD10. The sign of daily mean temperature bias tends to vary between CaRD10 and NNR between January and August without much consistency. The most notable systematic bias which appeared in both CaRD10 and NNR is the positive bias in minimum temperature in January which reduces the daily temperature range.

The daily temperature ranges in summer and winter are compared with a large number of land stations in 1996 and are shown in Figure 2 (the National Weather Service Cooperative Observer Program observations were provided courtesy of Mary Tyree). The geographical patterns look fairly reasonable for both January and July but CaRD10 tends to underestimate the temperature range, particularly in January.

3.2 Hourly scale

We compared the CaRD10 wind speeds with buoy observations on hourly scale by compositing the monthly diurnal variation from two years (2000-01) of data. We show the comparison at station b25, which is located to the south of Point of Conception, where the winds tend to be more variable than at other buoys (Figure 3). We see that the agreement of the CaRD10 diurnal cycle with observation is reasonably good, but CaRD10 shows larger diurnal amplitude. Similar agreement of diurnal cycle between CaRD10 and observations is found at other stations, but the amplitude difference varies significantly among stations.

Another example of the composite of the diurnal variation of winds is shown in Figure 4. This is the one month CaRD10 wind time-height composite compared with the observed composite taken from the special observation at Piedras Blancas (Ralph et al., 2000, this particular figure is provided courtesy of Paul Neiman). The observation is based on the hourly wind profiling radar deployed by NOAA. The timing of the diurnal variation of low level wind speed is very well represented by CaRD10, although the variability tends to be lower (6.5 m s^{-1} in observation v.s. 4.5 m s^{-1} in CaRD10). The variation of CaRD10 wind direction is fairly reasonable at around 1000m above ground, but tends to be too large near the surface.

Overall, diurnal variation is fairly reasonably reproduced by the downscaling, although evaluation of the accuracy may require further study.

3.3. Synoptic examples

Comparison of the dynamically downscaled analysis with station observation in terms of correlation, RMSE, and bias is not sufficient to demonstrate the meteorological

quality of the downscaled analysis. The integrity of CaRD10 can be more clearly demonstrated by showing examples of synoptic events. Here, we present one typical meso-scale example of the Catalina Eddy.

The Catalina Eddy is well documented by Wakimoto (1987) and Mass and Albright (1989). We took a typical case from Mass and Albright (their Fig. 2a) and examined the surface wind field from CaRD10. As shown in Figure 5, the dynamically downscaled analysis detects the eddy at a reasonable location, demonstrating the capability of the dynamical downscaling. Two discontinuity-like features in wind direction, one starting at Point Conception and the other extending from the south central region of the eddy toward the west-south-west direction are undocumented and worth further study.

We also examined coastally trapped wind reversal (CTWR) and Santa Ana events (see Part 2 for more detail) and found that the CaRD10 performs excellently in reproducing meso-scale features and its time evolutions. Although these are limited examples, it is clear that dynamical downscaling is capable of reproducing synoptically consistent small scale details over ocean and land.

3.4. Monthly averages

Validation of monthly average daily mean and maximum temperature, and precipitation over land was performed using about 80 United States Historical Climatology Network land stations during 1948-96. The monthly average data are more easily available than the daily data and thus we have more observations available for comparison. We show the fit of CaRD10 to these observations in January and August in Figure 6. The monthly mean 2-meter temperature in January correlates very well, above

0.7 over the entire domain (Fig. 6a). The correlation tends to be better along the southern coast of California than inland. The correlation in August is lower by 0.1 compared to January. In August the correlation tends to be lower along the coast and becomes better towards inland. The correlation stays above 0.6 over the entire domain. The reason for this geographical distribution of the CaRD10 temperature skill is not very clear, but some influence from ocean temperature is suspected. Our preliminary investigation showed that the CaRD10 temperature for coastal land in summer correlates more weakly with coastal SST than observed. This dominant local response over land in CaRD10 may be responsible for the poorer fit of temperature in August. This problem may be due to the over-estimated effect of land surface atmosphere interaction in the model. For the daily maximum temperature (not shown) during January, correlation is mostly over 0.7. The lowest correlation occurs in the Central Valley area where the value is in the 0.6 range or lower, but other areas have very high correlations. During August, the correlation tends to be lower, particularly in the southern half of the domain.

The correlations of monthly average precipitation are shown in Figure 6b and Table 6. During January, correlation is fairly high in most of California, while it is lower in Nevada where less precipitation occurs. During the summer, correlation is much lower (less than 0.6) over most of the domain. This is partly due to the lack of precipitation during this period.

The comparison of area averaged correlation between CaRD10 and NNR is shown in Table 7. We found that only daily mean and max temperature in January score better than NNR. This disappointing result seems to be a sampling problem. As discussed in more detail in section 4, when precipitation skill is computed using the

gridded observation, we found that there is a considerable small scale geographical variability in the temporal correlation (Fig. 10c and d). There are areas of low skill to the east of the Sierras in CaRD10, while the skill of NNR is smoothed out and retains only larger scale without areas of low skill. This geographical distribution resulted in lower area average skill for CaRD10 than for NNR. A similar feature is expected for the near surface temperature although we cannot verify this since we do not have an independent near surface temperature analysis like PRISM for precipitation. We believe that fine geographical structure of high and low skill is more useful than moderate skill at coarse resolution. From this point of view, any comparison of area average skill between coarse resolution and fine resolution models needs careful interpretation.

The monthly variation of correlation of daily mean near surface temperature at selected coastal (3 stations), valley (6 stations) and mountain (2 stations) locations (Table 2.b and Fig.1) is shown in Figure 7. The coastal stations display high correlation in winter months but very poor correlation during the summer. For the stations in the Central Valley, correlation is high in spring and fall, and lower again in summer, but not as low as the coastal stations. Mountain station skill is mixed. For the monthly mean precipitation (not shown), the correlation is better in winter over all stations (correlation of near 0.9) except stations v6 and m2 (correlation near 0.5). It is worse in summer, about 0.5 at stations c1, c2, v2, v3 and m1 but lower at other stations, again reflecting few precipitation events in summer.

3.5. Long-term Linear Trend

For validation of longer time scales, we examined the linear trends for the 1950-96 period at several selected stations (see Table 2.b and Fig. 1 for the station locations).

The linear trend was computed by the least square fit. Table 8 shows the comparison for the January and August trends. In January, the CaRD10 and observation trends agree fairly well, although the magnitude of the trend in the CaRD10 is consistently smaller (except mountain station m1). All the trends in the observation are positive, while CaRD10 shows a small negative trend in the valley at some stations. The statistical significance test showed that some of the positive trends in observation are significant, while positive trends in CaRD10 do not pass the test with the exception of station m1. In August, the CaRD10 trend does not agree with observation at all. Observed trends are all positive, while the CaRD10 trends are all negative with the exception of the mountain stations. More than half of the observed stations pass the statistical test of positive trend while negative trends in CaRD10 are statistically significant at all stations except one. This disagreement of CaRD10 with observation in summer needs to be examined in detail. Preliminary research suggests several causes: One possible cause is that the current downscaling does not take into account changes in land use, irrigation and urbanization, or changes in green house gasses and aerosol. The second is that the land surface processes affect near surface temperature too strongly in the model. Another possible reason is the effect of poorly analyzed coastal sea surface temperature with a cooling trend affecting the long term temperature trend over land.

Figure 8 shows the geographical distribution of linear trends of near surface temperature in CaRD10 for January and July. In January, the warm trend is apparent over most of the land region. The positive trend is greatest over the Sierra Nevada range and over Northern California/Oregon. The Central Valley displays weak or no trend. During July, most of the area shows a negative trend with a slight positive over the

Sierras and part of Nevada. There is a strong cooling trend in coastal ocean surface temperature, which seems to have some influence on the negative trend in the Central Valley. The impact of coastal SST on California has not been well documented. Further study of the possible problem of SST used in CaRD10 is warranted. There is a strong month-to-month variability in the linear trend.

As the last demonstration of the validation of decadal variability, the seasonal variation of monthly mean precipitation at 11 coastal, central and mountain stations (Table 2.b and Figure 1) are compared between two periods, 1950-74 and 1975-96. We observed a clear shift in the CaRD10 maximum precipitation month from Dec.-Jan. during the 1950-74 period to Jan.-Mar. during the 1975-96 period (Figure 9, lines with circles). Similar shifts were found in the observations (Fig. 9, thick lines without circles). This shift is consistent with the trend in earlier streamflow timing discussed by Stewart et al (2005). We also performed a statistical significance test of the time series of difference between February-March precipitation and December-January precipitation during the two periods, 1950-74 and 1975-96, and found that 8 stations out of 11 in observation and 9 out of 11 in CaRD10 have a statistically significant shift in precipitation months between these periods. Although this is just a simple demonstration, the CaRD10 is capable of reproducing decadal variability in the seasonal variation of precipitation.

4. Comparison with gridded precipitation analyses

The validation of precipitation against station observation is problematic due to measurement error and the representativeness of the observation. We try to overcome this problem by using high resolution gridded precipitation analysis. We utilized two products, PRISM and Higgins analysis. The PRISM (Daly et al., 1994, 2001, 2002) is a

method to analyze small scale precipitation distribution over complex topography by combining various information such as distance, elevation, cluster, vertical layer, topographic facet, coastal proximity, and effective terrain. For PRISM, only monthly average analyses were available and we used them for validating monthly average and long term trend. Higgins analysis (Higgins et al 2000) is based on modified Cressman successive-scan analysis technique, and is available daily on 1/8 degree grid. We utilized this analysis for computing threat and bias scores of the daily CaRD10 precipitation.

Figure 10a,b compares the bias of monthly climatology (January and August for 1950-97) against the PRISM analysis for CaRD10 and NNR. It is apparent that the bias in CaRD10 is large, exceeding 9 mm day^{-1} in some places. Large positive bias is primarily found on the windward side of the Sierras and large negative bias is found on the lee side of the Sierras. It is noted that the NNR bias is much smaller, but the lack of small scale detail makes it difficult to judge the quality of the analysis.

Equitable threat scores (Schaefer, 1990) and bias scores are standard measures of the precipitation skill of the model. The equitable threat score is defined as

$$\frac{H - CH}{F + O - H - CH}$$

where F is the number of grid points that forecast more than the precipitation threshold. O is the number of grid points that observe more than the threshold. H is the number of grid points that correctly forecast more than the threshold. CH is the expected number of correct forecasts due to chance (F*O/T) where T is the total number of grid points inside the verification domain. The best bias score is 1.0. Scores above (below) 1.0 indicate wet (dry) bias of precipitation forecast.

Table 9 shows the daily CaRD10 precipitation skill score during January and August, 1998. Higgins gridded precipitation analysis is used as observation to compute the threat and bias scores. CaRD10 shows the best threat score at the threshold of 2 mm day^{-1}. The CarD10 bias score is reasonable for smaller precipitation thresholds, but a wet bias is apparent in larger precipitation thresholds. These scores suggest that CaRD10 precipitation in January covers reasonable spatial extent as a whole, but too much precipitation occurs in the wrong places. August precipitation is small and CaRD10 shows no skill in the threat score. Bias scores suggest that CaRD10 is too dry in August.

Figure 10c,d is the temporal correlation of CaRD10 monthly averaged precipitation against the PRISM analysis in January, computed for the 1950-97 period. The CaRD10 correlation over the state of California is generally above 0.7, which agrees with the correlation against station observation shown in Fig. 6. The correlation is particularly low on the lee side of the Sierra Nevada. This is likely due to the lack of cloud water prediction in this version of the model, which prevents advection of cloud water to the lee side of the mountains, causing difficulties in reproducing precipitation spreading to the east of high mountain ranges. The correlation of precipitation in the NNR is quite respectable, considering its coarse horizontal resolution. The summer correlation is much lower (not shown), because precipitation events are very scarce in this season.

Finally, the 1950-97 trend in precipitation is compared between PRISM and CaRD10, as shown in Figure 11. Both patterns agree quite well, with much more small scale detail in CaRD10. The tendency of increased precipitation in the south and reduced precipitation along the northern California/Oregon coast stands out. The negative

tendency along the high Sierra Nevada is very clear in CaRD10, and some hint of it is seen in PRISM.

In summary, the comparison with gridded precipitation analysis indicated that the CaRD10 is reasonable in reproducing daily and year-to-year variation of monthly mean precipitation, as well as its long term trend. However, the absolute amount of precipitation has a positive bias for heavy precipitation regions for daily time scale and the windward side of high mountains for monthly time scale. These conclusions agree well with the CaRD10 comparison with station observations.

A recent experiment showed that the overestimation of precipitation is related to the relaxed Arakawa Schubert convective parameterization used in CaRD10. This parameterization was originally designed for use in coarser resolution global models, and was shown to perform excellently. However, the parameterization tends to overestimate precipitation in a high resolution model. A test run with Kain-Fritsch convective parameterization scheme (Kain and Fritsch, 1993) with prediction of cloud water (Zhao and Carr, 1997) significantly reduced the wet bias over the CaRD10 domain.

5. Conclusions

The dynamical downscaling of NCEP-NCAR global reanalysis is performed over the state of California and the neighboring states and ocean. The horizontal resolution of the regional model is 10 km and the output is produced every hour. The integration period covers 57 years, from 1948 to 2005. The SSBC is applied to reduce the error of the scale greater than 1000 km.

Comprehensive validation of the downscaled analyses is performed using available buoy observations over coastal ocean and various land stations. CaRD10 is also compared with the large scale boundary forcing (NNR) to make sure that the regional downscaling does provide regional scale information more accurately than the NNR. In addition, comparison is made with the gridded precipitation analysis to further ensure the quality of the product. These validations are separately performed for hourly, daily, monthly and decadal scales.

In general, the quality of the downscaled product is reasonably high. The product is definitely better than the coarse resolution NNR. There is a large difference in the quality between winter and summer, winter being better. The winds over coastal ocean are significantly improved by downscaling. Over land, the accuracy of CaRD10 near surface winds and temperature are good due to the finer topography resolved by the CaRD10. The examination of typical meso-scale events, namely the Catalina Eddy, Coastally Trapped Wind Reversal and Santa Ana showed that the downscaling reproduces characteristic features very well. There are some differences in the skill of the CaRD10 for daily and monthly mean time scales. The monthly mean skill of temperature is generally higher in January, but lower in August than that of daily mean skill. The long term trend of near surface temperature obtained from 1950-96 agrees fairly well with station observation in January, but the trend is underestimated. In August the trend is negative over a large part of the domain in CaRD10 while it is positive in the station observation. This discrepancy is likely the result of poor representation of land process in the model, inaccuracies in the coastal sea surface temperature, and the use of climatology of land surface characteristics and atmospheric compositions in CaRD10.

The precipitation skill against station observation showed that the correlation is reasonable on the order of 0.6-0.8 on the monthly scale. However, there is a noticeable positive bias in large precipitation events. Comparison with gridded analysis revealed that the CaRD10 daily time scale precipitation area with more than 10 mm day^{-1} can be 1.5 times larger than that of the observation. Although the gridded analysis cannot be fully trusted, particularly over complex terrain, it is likely that CaRD10 overestimated the precipitation. The 1950-97 linear trend, however, agrees very well between CaRD10 and PRISM. These precipitation validations suggest that although the absolute magnitude of the precipitation may be problematic, the long term trend, year-to-year variation, and probably day-to-day variation are reasonably good and can be used for climate research if we are sufficiently cautious.

The advantage of dynamical downscaling over statistical downscaling is that all variables in the downscaled analysis are dynamically, physically and hydrologically consistent, at least within the framework of the downscaling system. Thus, the downscaled analysis provides ways to study various regional phenomena of widely ranging time scales in a consistent manner. However, it is important to understand the limitations of downscaled analysis before it is used for those studies.

The results of more detailed validation of the CaRD10 are documented in Kanamitsu and Kanamaru (2006) which interested parties are encouraged to read. Part 2 of this paper describes an in-depth comparison of CaRD10 against NARR. The CaRD10 dataset is currently available in-house at the Scripps Institution of Oceanography and web access of the entire dataset is available to general public (http://cec.sdsc.edu). The data can also be obtained by writing to the authors.

Acknowledgements

This work was funded by the California Energy Commission Public Interest Energy Research (PIER) program, which supports the California Climate Change Center (Award Number MGC-04-04). The authors sincerely thank G. Franco for his assistance in performing this research. We would also like to thank Dr. Dan Cayan for continuous encouragement throughout this study. We also thank Drs. Henry Juang and Yi-Feng Cui for converting the regional code to parallel machine. Without their contribution, this project would not have been possible. We also thank Ms. Mary Tyree and Mr. Steve Taylor for providing observational data, and Drs. Marty Ralph and Paul Neiman for providing observational diurnal variation data from Piedras Blancas. The computations were performed at the National Center for Atmospheric Research, the San Diego Supercomputer Center, and the University of Illinois National Center for Supercomputing Applications. The assistance of Ms. Diane Boomer in refining the writing is appreciated.

References

Alpert, J.C., M. Kanamitsu, P.M. Caplan, J.G. Sela, G.H. White, and E. Kalnay, 1988: Mountain induced gravity wave drag parameterization in the NMC medium-range model. Preprints of the Eighth Conference on Numerical Weather Prediction, Baltimore, MD, American Meteorological Society, 726-733.

Archer, C. L., and M. Z. Jacobson, 2003: Spatial and temporal distributions of U.S. winds and wind power at 80m derived from measurements. *J. Geophys. Res.*, **108**, 4289, doi:10.1029/2002JD002076.

Breaker, L. C., W. H. Gemmil and D. S. Crosby, 1994: The Application of a Technique for Vector Correlation to problems in Meteorology and Oceanography. *J. Appl. Met.*, **33**, 1354-1365.

Chen, F. and Coauthors, 1996: Modeling of land surface evaporation by four schemes and comparison with FIFE observations. *J. Geophys. Res.*, **101**, 7251-7268.

------, and J. Dudhia 2001a: Coupling an advanced land -surface hydrology model with the Penn States/NCAR MM5 modeling system. Part I: Model implementation and sensitivity. *Mon. Wea. Rev.*, **129**, 569-585.

------, and ------- 2001b: Coupling an advanced land -surface hydrology model with the Penn States/NCAR MM5 modeling system. Part II: Preliminary model validation. *Mon. Wea. Rev.*, **129**, 587-604.

Chou, M.-D. and M. J. Suarez, 1994: An efficient thermal infrared radiation parameterization for use in General Circulation Models. Technical Report Series on Global Modeling and Data Assimilation, National Aeronautical and Space Administration/TM-1994-104606, 3, 85 pp.

------, and K.-T. Lee, 1996: Parameterizations for the absorption of solar radiation by water vapor and ozone. *J. Atmos. Sci.*, **53**, 1203-1208.

Daly, C., R.P. Neilson,, and ,D.L. Phillips 1994: A Statistical-Topographic Model for Mapping Climatological Precipitation over Mountainous Terrain. *J. Appl. Met.*, **33**, 140–158.

------, Taylor, G.H., W.P. Gibson, T.W. Parzybok, G.L. Johnsonn, and P Pasteris,. 2001: High-quality spatial climate data sets for the United States and beyond. *Transactions of the American Society of Agricultural Engineers*, **43**, 1957–1962.

------, Gibson, W.P., G.H. Taylor,, G.L. Johnson,, and P Pasteris,. 2002. A knowledge-based approach to the statistical mapping of climate. *Climate Research*, **22**, 99–113.

------, Helmer, E.H., and M. Quinones, 2003: Mapping the climate of Puerto Rico, Vieques and Culebra. *International Journal of Climatology*, **23**, 1359–1381.

Fiorino, M., 2004: A Multi-decadal Daily Sea Surface Temperature and Sea Ice Concentration Data Set for the ERA-40 Reanalysis. ERA-40 project Report Series. ECMWF, Shinfield Park, Reading, RG2 9AX, UK. 16pp.

Higgins, R. W., W. Shi, E. Yarosh and R. Joyce, 2000: Improved United States precipitation Quality control system and analysis. NCEP/Climate Prediction Center Atlas No. 7, U.S. Department of Commerce. [Available at: http://www.cpc.mcep.npoaa.gov/research_papers/ncep_cpc_atlas/7/index.html]

Hong, S.-Y., H.-L. Pan, 1996: Nonlocal Boundary Layer Vertical Diffusion in a Medium-Range Forecast Model. *Mon. Wea. Rev.*, **124**, 2322-2339.

Juang, H.-M. and S.-Y. Hong, 2001: Sensitivity of the NCEP Regional Spectral Model to Domain Size and Nesting Strategy. *Mon. Wea. Rev.* **129**, 2904–2922, DOI: 10.1175/1520-0493(2001)129<2904:SOTNRS>2.0.CO;2

------, and M. Kanamitsu, 1994: The NMC nested regional spectral model. *Mon. Wea. Rev*., **122**, 3-26.

Kalnay, E., and Coauthors, 1996: The NCEP/NCAR 40-year reanalysis project. *Bull. Amer. Met. Soc.*, **77**, 437-471.

Kanamaru H. and M. Kanamitsu, 2006: Scale-Selective Bias-Correction in a Downscaling of Global Analysis Using a Regional Model. *Mon. Wea. Rev.*, in press.

Kanamitsu, M. and K. Mo, 2003: Dynamical Effect of Land Surface Processes on Summer precipitation over the Southwestern United States. *J. Climate*, **16**, 496-509.

------, and H. Kanamaru. 2006. *Fifty-Seven Year California Reanalysis Downscaling at 10 Kilometers (CaRD10).* Available from http://www.climatechange.ca.gov/documents/pier_gcc_reports.html

------, W. Ebisuzaki, J. Woollen, S.-K. Yang, J. Hnilo, M. Fiorino, and J. Potter, 2002: NCEP/DOE AMIP-II REANALYSIS (R-2). *Bull. Amer. Met. Soc.* **83**, 1631-1643.

------, H. Kanamaru, Y. Cui and H. Juang. 2005: Parallel Implementation of the Regional Spectral Atmospheric Model. CEC-500-2005-014. Available from http://www.energy.ca.gov/2005publications/CEC-500-2005-014/CEC-500-2005-014.PDF

Keely, J. E., C. J. Fotheringham and M. Moritz, 2004: Lessons from the October 2003 Wildfires in Southern California. *Journal of Forestry,* **102**, 26-31.

Koepke, P., M. Hess, I. Schult, and E.P. Shettle, 1997: Global aerosol data set. MPI Meteorologie Hamburg Report No. 243, 44 pp.

Mass, C. F. and M. D. Albright, 1989: Origin of the Catalina Eddy, *Mon. Wea. Rev.*, **117**, 2406-2436.

Mesinger, F., Geoff DiMego, Eugenia Kalnay, Kenneth Mitchell, Perry C. Shafran, Wesley Ebisuzaki, Dusan Jovic, Jack Woollen, Eric Rogers, Ernesto H. Berbery, Michael B. Ek, Yun Fan, Robert Grumbine, Wayne Higgins, Hong Li, Ying Lin, Geoff Manikin, David Parrish, and Wei Shi, 2006: NORTH AMERICAN REGIONAL REANALYSIS. *Bull. Amer. Met. Soc.* **87**, 343-360.

Mitchell, K., C. and Coauthors, 2000: The collaborative GCIP land data assimilation (LDAS) project and supportive NCEP uncoupled land-surface modeling Initiatives. Preprints, 15th Conf. On Hydrology, Amer. Meteor. Soc., Long Beach, CA, 1-4.

Moorthi, S., and M. J. Suarez, 1992: Relaxed Arakawa-Schubert: A parameterization of moist convection for general circulation models. *Mon. Wea. Rev.*, **120**, 978-1002.

Mo, K. C., M. Chelliah, M. L. Carrera, R. W. Higgins and W. Ebisuzaki, 2005: Atmospheric Moisture Transport over the United States and Mexico as Evaluated in the NCEP Regional Reanalysis. *J. Hydromet.* **6**, 710–728.

Nuss, W. A., J,. M. Bane, W. T. Thompson, T. Holt, C/ W. Dorman F. M. Ralph, R. Rotunno, J. B. Klemp, W. C. Skamarock, R. M. Jackson. A. M. Rogerson, C.

Reason and P. Jackson, 2000: Coastally Trapped Wind Reversals: Progress toward Understanding. *Bull. Amer. Met. Soc*., **81**, 719-743.

Orszag, S. A., 1970: Transform method for calculation of vector coupled sums: Application to the spectral form of the vorticity equation. *J. Atmos. Sci*., **27**, 890-895.

Pan, H.-L. and L. Mahrt, 1987: Interaction between soil hydrology and boundary layer developments. *Boundary Layer Meteor.*, **38**, 185-202.

Qian, J.-H. Anji Seth, and Stephen Zebiak, 2003: Reinitialized versus Continuous Simulations for Regional Climate Downscaling. *Mon. Wea. Rev*., **131**, 2857-2874.

Ralph, F. M., P. J. Neiman, P. O. G. Persson, J. M. Bane, M. L. Cancillo, J. M. Wilczak and W. Nuss. 2000: Kelvin Waves and Internal Bores in the Marine Boundary Layer Inversion and Their Relationship to Coastally Trapped Wind Reversals. *Mon. Wea. Rev.*, **128**, 283–300.

Roads, J. O., S.-C. Chen and M. Kanamitsu, 2003: U.S. regional climate simulations and seasonal forecasts. *J. Geophys. Res*., **108**, 8606, doi10.1029/2002JD002232.

Robertson, A.W., Upmanu Lall, Stephen E. Zebiak and Lisa Goddard. 2004: Improved Combination of Multiple Atmospheric GCM Ensembles for Seasonal Prediction. *Mon. Wea. Rev.*, **132,** 2732–2744.

Schaefer, J. T., 1990: The critical success index as an indicator of warning skill. *Wea. Forecasting*, **5**, 570-575.

Slingo, J.M., 1987: The development and verification of a cloud prediction model for the ECMWF model. *Quart. J. Roy. Meteor. Soc*., **113**, 899-927.

Stewart, I.T., D.R. Cayan and M.D. Dettinger, 2005: Changes toward earlier streamflow timing across Western North America. *J. Climate,* **18**, 1136-1155.

Taylor, K. E., D. Williamson, and F. Zwiers, 2000: The sea surface temperature and sea-ice concentration boundary conditions of AMIP II simulations. PCMDI report #60, 20pp.

Tiedtke, M., 1983: The sensitivity of the time-mean large-scale flow to cumulus convection in the ECMWF model. Proceedings of the ECMWF Workshop on Convection in Large-Scale Models, 28 November-1 December 1983, European Centre for Medium-Range Weather Forecasts, Reading, England, 297-316.

von Storch, H., H. Langenberg, and F. Feser, 2000: A spectral nudging technique for dynamical downscaling purposes, *Mon. Wea. Rev.*, **128**, 3664-3673.

Wakimoto, R. M., 1987: The Catalina Eddy and its Effect on Pollution over Southern California. *Mon. Wea. Rev.,* **115**, 837-855.

Williamson, D. L., 2002: Time-Split versus Process-Split Coupling of Parameterizations and Dynamical Core. *Mon. Wea. Rev.*, **130**, 2024-2041.

Figure captions

Figure 1. CaRD10 domain, surface elevation (m), and observation station locations used in CaRD10 validation. Buoy observation stations are indicated by blue circles (names begin with "b," courtesy of Steve Taylor). The USHCN stations are indicated by black squares (names begin with "c," "v," or "m") and the NCDC stations are indicated by red "cross-hairs" (three-letter abbreviations).

Figure 2. Comparison of daily temperature range for January (top panels) and July (bottom panels) 1996. Left panels are observation (courtesy of Mary Tyree), and right panels are CaRD10.

Figure 3. Comparison of monthly mean diurnal variation of near surface winds for the average of 2000 and 2001 at buoy station b25. Mean daily wind is subtracted and only anomaly is plotted. Solid line is buoy observation and dashed line is CaRD10. X axis is time (UTC) and Y axis is wind speed (m s^{-1}).

Figure 4. Validation of composite diurnal variation of wind speed and direction at Piedras Blancas (35.7N, 121.3W) for the period June 24 to July 21, 1996. Left panel is observation (from Fig. 9 in Ralph et al. (2000); courtesy of Paul Neiman). Y axis is in meters. Right panel is CaRD10. Y axis is in hPa. Contour is wind speed in m s^{-1}. Half barb = 2.5 m s^{-1} and full barb=5.0 m s^{-1}.

Figure 5. An example of the Catalina Eddy as it appeared in the CaRD10 at 1500UTC, May 22, 1984. Shades and arrows indicate winds at 10m above surface (m s^{-1}).

Figure 6. Correlation of monthly average of a) daily mean temperature and b) precipitation with observation for the period 1948-96.

Figure 7. Variation of correlation of monthly mean temperature with observation for the period 1948-96 at coastal (c1 to c3), Central Valley (v1 to v6) and mountain (m1 and m2) stations.

Figure 8. 1950-96 linear trend of 2-meter temperature (K $year^{-1}$) for January (left) and July (right) in CaRD10.

Figure 9. Seasonal variation of monthly averaged precipitation (mm day^{-1})in CaRD10 at 11 selected observation locations. 1950-74 climatology and 1975-96 climatology are plotted separately.

Figure 10. January mean precipitation comparison of CaRD10 and NNR against PRISM analysis for the 1950-97 period. Bias a) in CaRD10 and b) in NNR. Unit mm day^{-1}. Temporal correlations c) in CaRD10 and d) in NNR.

Figure 11. Comparison of the 1950-97 trend in January mean precipitation rate. a) PRISM and b) CaRD10. Unit is in mm day^{-1} $decade^{-1}$.

Table 1. Physics of the Regional Spectral Model.

	Parameterization	Reference
Convection	Relaxed Arakawa Schubert	Moorthi and Suarez (1992)
Large scale condensation	Evaporation of rain included	
Shallow Convection	Tiedtke scheme	Tiedtke (1983)
Boundary Layer	Non-Local scheme	Hong and Pan (1996)
Surface Layer	Monin-Obukhov	
Long wave radiation	M.-D. Chou	Chou and Suarez (1994)
Short wave radiation	M.-D. Chou	Chou and Lee (1996)
Cloud	Slingo	Slingo (1987)
Gravity wave drag	Pierrhumbert	Alpert et al (1988)
Vertical Diffusion	Richardson number dependent	
Land model	OSU	Pan and Mahrt (1987)
Land characteristics	USGS	
Direct evaporation	NCAR	Chen (1996)
Topography	Smoothed mean from USGS GTOPO30	

Table 2a. Buoy station locations

WMO ID	Sign	Location	Latitude	Longitude
46011	b11	Santa Maria	34.88 N	120.87 W
46012	b12	Half Moon Bay	37.36 N	122.88 W
46013	b13	Bodega Bay	38.23 N	123.32 W
46014	b14	Pt. Arena	39.22 N	123.97 W
46022	b22	Eel River	40.78 N	124.54 W
46023	b23	Pt. Arguello	34.71 N	120.97 W
46025	b25	Santa Monica Basin	33.75 N	119.08 W
46026	b26	San Francisco	37.75 N	122.82 W
46028	b28	Cape San Martin	35.74 N	121.89 W
46042	b42	Monterey	36.75 N	122.42 W
46047	b47	Tanner Banks	32.43 N	119.53 W
46053	b53	Santa Barbara E	34.24 N	119.85 W
46054	b54	Santa Barbara W	34.27 N	120.45 W
46062	b62	Pt. San Luis	35.10 N	121.01 W
46063	b63	Pt. Conception	34.27 N	120.66 W

Table 2b. Stations for monthly analysis (data obtained from United States Historical Climatology Network).

COOP ID	**Sign**	**Location**	**Latitude**	**Longitude**
042910	c1	Eureka WSO	40.80 N	124.17 W
047916	c2	Santa Cruz	36.98 N	122.02 W
046175	c3	Newport Beach Harbor	33.60 N	117.88 W
046506	v1	Orland	39.75 N	122.20 W
045385	v2	Marysville	39.15 N	121.60 W
042294	v3	Davis Exp Farm	38.53 N	121.77 W
043257	v4	Fresno WSO AP	36.78 N	119.72 W
043747	v5	Hanford	36.30 N	119.65 W
049452	v6	Wasco	35.60 N	119.33 W
044713	m1	Lake Spaulding	39.32 N	120.63 W
048758	m2	Tahoe City	39.17 N	120.13 W

Table 2c. Airport stations for daily analysis (data obtained from NCDC).

COOP ID	**Sign**	**Location**	**Latitude**	**Longitude**
040442	BFL	Bakersfield	35.43 N	119.05 W
040822	BIH	Bishop	37.37 N	118.35 W
045115	CQT	Los Angeles USC	34.02 N	118.28 W
043257	FAT	Fresno	36.77 N	119.72 W
045114	LAX	Los Angeles	33.93 N	118.40 W
045085	LGB	Long Beach	33.82 N	118.15 W
047304	RDD	Redding	40.50 N	122.30 W
047630	SAC	Sacramento	38.50 N	121.48 W
047740	SAN	San Diego	32.73 N	117.17 W
048558	SCK	Stockton	37.88 N	121.23 W
047769	SFO	San Francisco	37.62 N	122.38 W
047946	SMX	Santa Maria	34.90 N	120.45W

Table 3. Vector anomaly correlation and RMSE of winds of two analyses and fifteen buoy observations during 2000. Better correlation and RMSE of the two are indicated in bold.

	January				August			
	Correlation		RMSE ($m\ s^{-1}$)		Correlation		RMSE ($m\ s^{-1}$)	
	CaRD10	NNR	CaRD10	NNR	CaRD10	NNR	CaRD10	NNR
b11	N/A	N/A	N/A	N/A	0.65	**0.66**	**1.48**	2.25
b12	N/A	N/A	N/A	N/A	**0.68**	0.62	**1.98**	2.54
b13	**0.94**	0.88	**2.70**	3.59	0.72	**0.74**	**2.20**	4.28
b14	**0.89**	0.82	**2.69**	3.15	**0.78**	0.69	**1.88**	2.50
b22	**0.91**	0.85	**3.17**	3.82	0.64	**0.65**	2.39	**2.26**
b23	0.73	**0.78**	3.89	**3.56**	**0.69**	0.64	**1.73**	2.11
b25	**0.77**	0.61	**2.77**	4.15	**0.58**	0.46	**1.27**	2.12
b26	**0.92**	0.86	**2.48**	3.07	**0.83**	0.68	**1.36**	2.50
b28	N/A	N/A	N/A	N/A	**0.73**	0.69	**2.21**	3.36
b42	**0.88**	0.78	**3.16**	4.03	**0.69**	0.65	**1.88**	3.13
b47	**0.93**	0.92	2.72	**2.65**	**0.78**	0.77	**1.40**	1.48
b53	**0.69**	0.61	**2.52**	3.84	0.54	**0.55**	**2.35**	2.58
b54	**0.66**	0.65	**3.57**	4.17	0.67	**0.73**	**2.03**	2.23
b62	**0.85**	0.84	2.71	**2.36**	**0.68**	0.64	**1.61**	1.98
b63	**0.69**	0.66	**2.91**	3.60	N/A	N/A	N/A	N/A
All station average	**0.82**	0.77	**2.94**	3.50	**0.69**	0.66	**1.84**	2.52

Table 4. Vector anomaly correlation and RMSE of winds of two analyses and twelve land station observations during 2000. Better correlation and RMSE of the two are indicated in bold.

	January				August			
	Correlation		RMSE (m s^{-1})		Correlation		RMSE (m s^{-1})	
	CaRD10	NNR	CaRD10	NNR	CaRD10	NNR	CaRD10	NNR
BFL	**0.43**	0.36	**2.33**	2.85	**0.53**	0.26	**1.59**	2.03
BIH	**0.49**	0.47	**3.45**	4.12	**0.43**	0.36	**4.00**	4.41
CQT	0.44	**0.44**	**2.29**	3.25	**0.28**	0.16	**0.96**	1.45
FAT	**0.59**	0.47	**2.94**	3.63	**0.41**	0.31	**1.72**	1.96
LAX	**0.54**	0.44	**2.81**	3.58	**0.41**	0.39	**1.62**	2.28
LGB	**0.58**	0.36	**2.63**	4.07	**0.38**	0.27	**2.35**	2.81
RDD	0.57	**0.64**	**4.18**	5.35	**0.52**	0.37	**1.52**	1.87
SAC	**0.64**	0.49	**3.52**	4.41	0.56	**0.61**	**2.34**	2.55
SAN	0.41	**0.52**	2.94	**2.87**	**0.47**	0.44	**2.68**	2.93
SCK	**0.60**	0.48	**3.73**	4.44	0.55	**0.57**	**2.39**	3.23
SFO	**0.78**	0.62	**4.12**	4.25	0.56	**0.56**	**4.53**	4.62
SMX	**0.63**	0.57	**4.01**	4.02	**0.48**	0.42	1.74	**1.28**
All station average	**0.56**	0.49	**3.24**	3.90	**0.46**	0.39	**2.29**	2.62

Table 5. Mean correlation, RMSE, and bias of daily mean temperature and max/min temperature of two analyses and twelve land station observations during 2000. Better fit of the two is indicated in bold. For the RMSE, mean value is subtracted at each station. For the mean bias, temperature is corrected for elevation with lapse rate of 6.5K km^{-1} and absolute values of bias at each station are averaged.

		Correlation		RMSE (K)		Bias (K)	
		CaRD10	NNR	CaRD10	NNR	CaRD10	NNR
Mean T	January	**0.77**	0.77	**1.66**	1.73	**0.52**	0.81
	August	**0.71**	0.67	**1.73**	1.74	**1.51**	2.59
Tmax	January	**0.47**	0.45	**2.37**	2.47	**0.50**	2.18
	August	**0.75**	0.75	2.45	**2.35**	**2.48**	4.72
Tmin	January	0.75	**0.77**	**2.47**	2.53	2.38	**1.98**
	August	**0.49**	0.40	**2.17**	2.25	2.19	**1.60**

Table 6. Correlation and bias (in mm day^{-1}) between CaRD10 and daily station observation of precipitation for 6 selected stations in California in January and August for the period 1948-2003.

	January		August	
Station	Corr.	Bias	Corr.	Bias
c2	0.68	1.00	0.50	0.08
c3	0.66	1.33	0.12	-0.02
v1	0.60	3.54	0.33	0.05
v3	0.60	2.43	0.14	0.06
v6	0.43	2.01	0.03	0.01
m1	0.84	1.04	0.40	0.10

Table 7. Correlation of monthly average of daily mean temperature, daily max temperature, and precipitation with observation for the period 1948-96. All station (Figure 6) values are averaged.

	January			August		
	Daily Mean Temperature	Daily Max Temperature	Precipitation	Daily Mean Temperature	Daily Max Temperature	Precipitation
CaRD10	**0.84**	**0.76**	0.69	0.68	0.69	0.57
NNR	0.78	0.65	**0.77**	**0.74**	**0.73**	**0.64**

Table 8. Comparison of 1950-96 trend in monthly mean near surface temperature (K decade^{-1}) between observation and CaRD10. Statistically significant (95% confidence) positive/negative trend is indicated in bold.

	Station	January		August	
		Obs.	CaRD10	Obs.	CaRD10
Coast	c1	**+0.04**	+0.02	**+0.04**	**-0.04**
	c2	**+0.05**	+0.02	**+0.03**	**-0.04**
	c3	**+0.07**	+0.02	**+0.05**	**-0.03**
Valley	v1	**+0.04**	+0.00	+0.00	**-0.04**
	v2	**+0.04**	+0.00	+0.02	**-0.04**
	v3	+0.01	-0.00	+0.01	**-0.03**
	v4	+0.02	+0.01	**+0.05**	**-0.05**
	v5	+0.02	-0.00	+0.01	**-0.05**
	v6	+0.02	-0.00	**+0.03**	**-0.05**
Mountain	m1	+0.04	**+0.06**	**+0.04**	+0.00
	m2	**+0.05**	+0.02	**+0.06**	**+0.25**

Table 9. Precipitation skill scores of CaRD10 in January 1998 with respect to gridded Higgins precipitation analysis (Higgins et al, 2000).

Threshold (mm day^{-1})	Threat score	Bias score
0.05	0.19	0.96
0.1	0.20	1.04
0.2	0.22	1.09
0.5	0.27	1.13
1	0.30	1.14
2	0.32	1.15
5	0.30	1.27
10	0.24	1.65

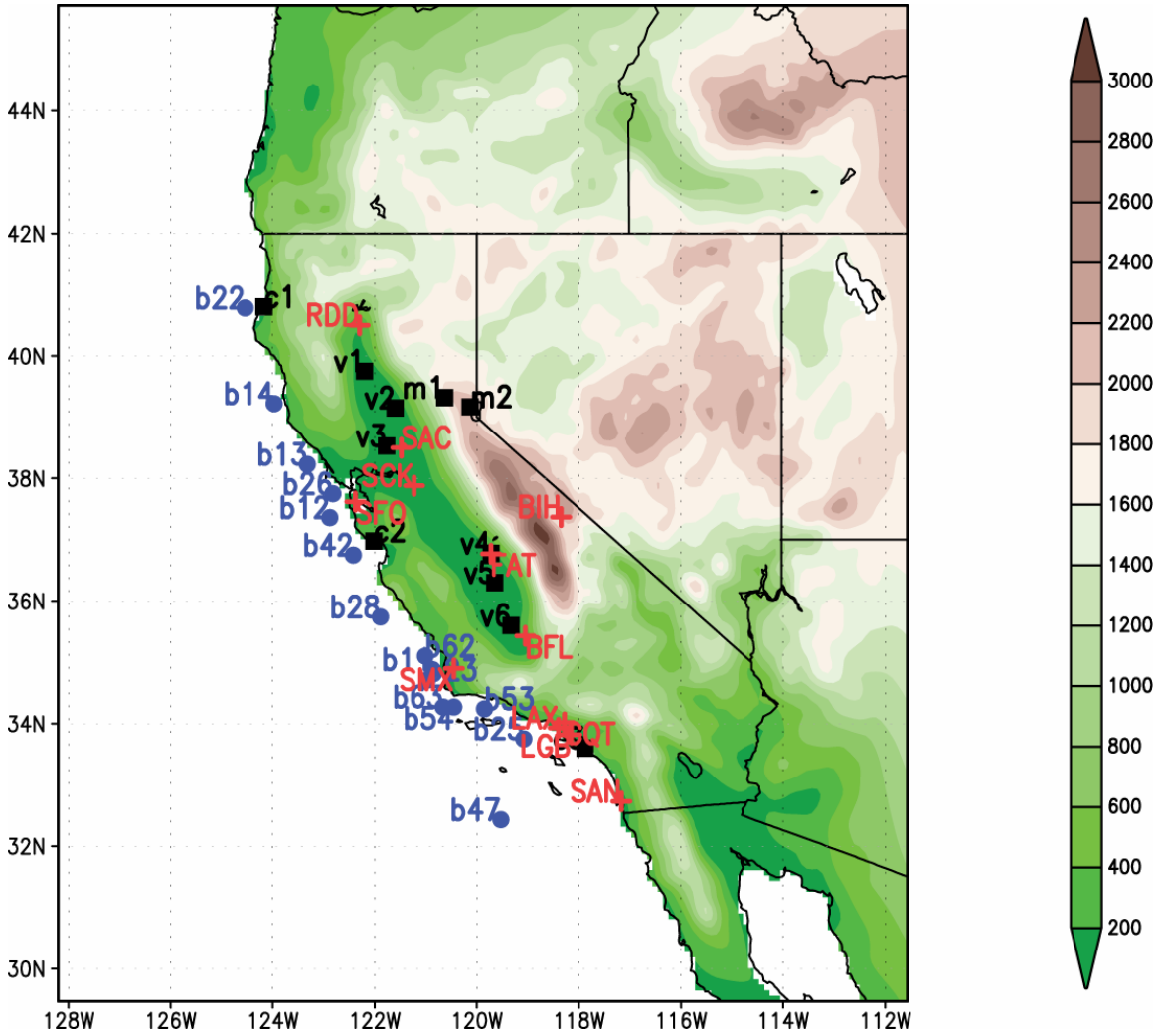

Figure 1. CaRD10 domain, surface elevation (m), and observation station locations used in CaRD10 validation. Buoy observation stations are indicated by blue circles (names begin with "b," courtesy of Steve Taylor). The USHCN stations are indicated by black squares (names begin with "c," "v," or "m") and the NCDC stations are indicated by red "cross-hairs" (three-letter abbreviations).

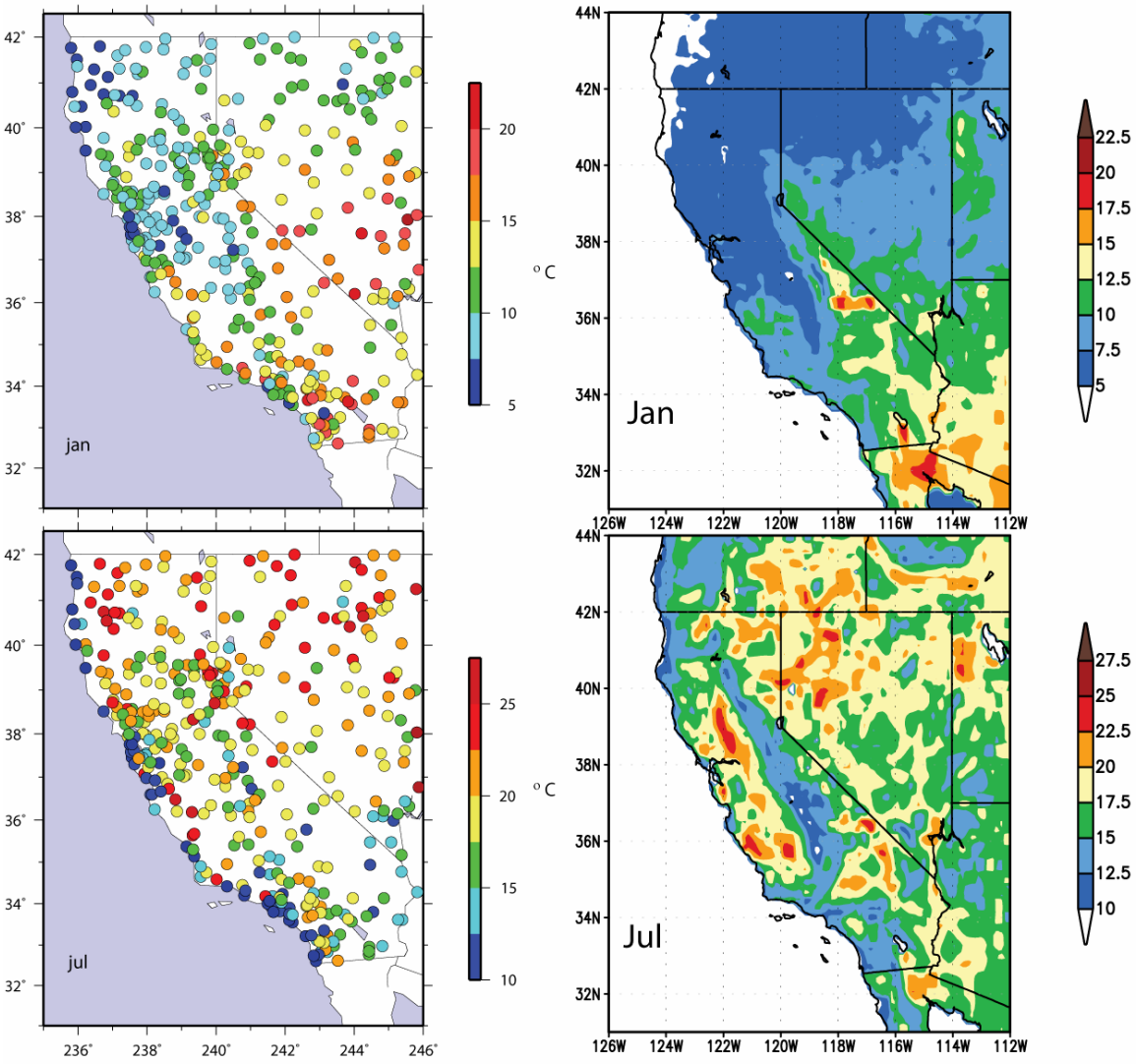

Figure 2. Comparison of daily temperature range for January (top panels) and July (bottom panels) 1996. Left panels are observation (courtesy of Mary Tyree), and right panels are CaRD10.

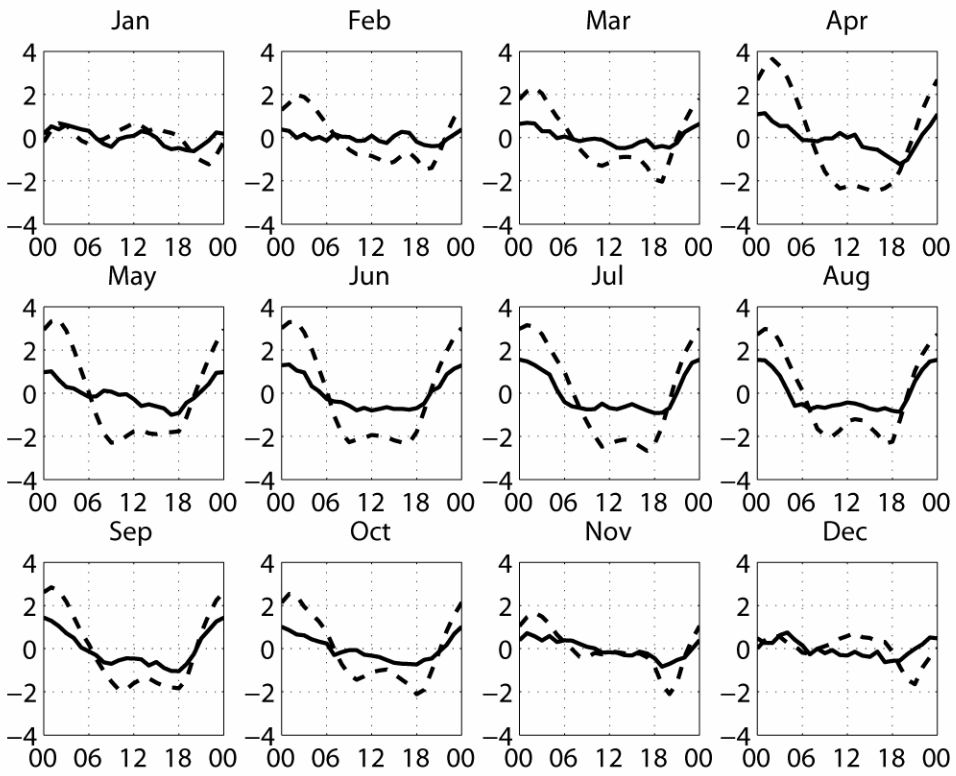

Figure 3. Comparison of monthly mean diurnal variation of near surface winds for the average of 2000 and 2001 at buoy station b25. Mean daily wind is subtracted and only anomaly is plotted. Solid line is buoy observation and dashed line is CaRD10. X axis is time (UTC) and Y axis is wind speed (m s^{-1}).

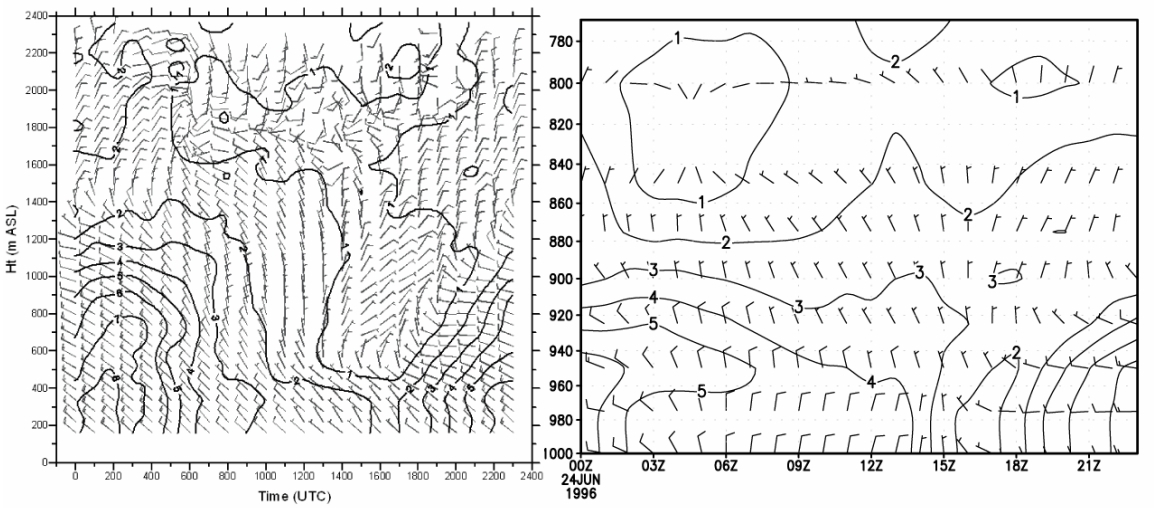

Figure 4. Validation of composite diurnal variation of wind speed and direction at Piedras Blancas (35.7N, 121.3W) for the period June 24 to July 21, 1996. Left panel is observation (from Fig. 9 in Ralph et al. (2000); courtesy of Paul Neiman). Y axis is in meters. Right panel is CaRD10. Y axis is in hPa. Contour is wind speed in m s^{-1}. Half barb = 2.5 m s^{-1} and full barb=5.0 m s^{-1}.

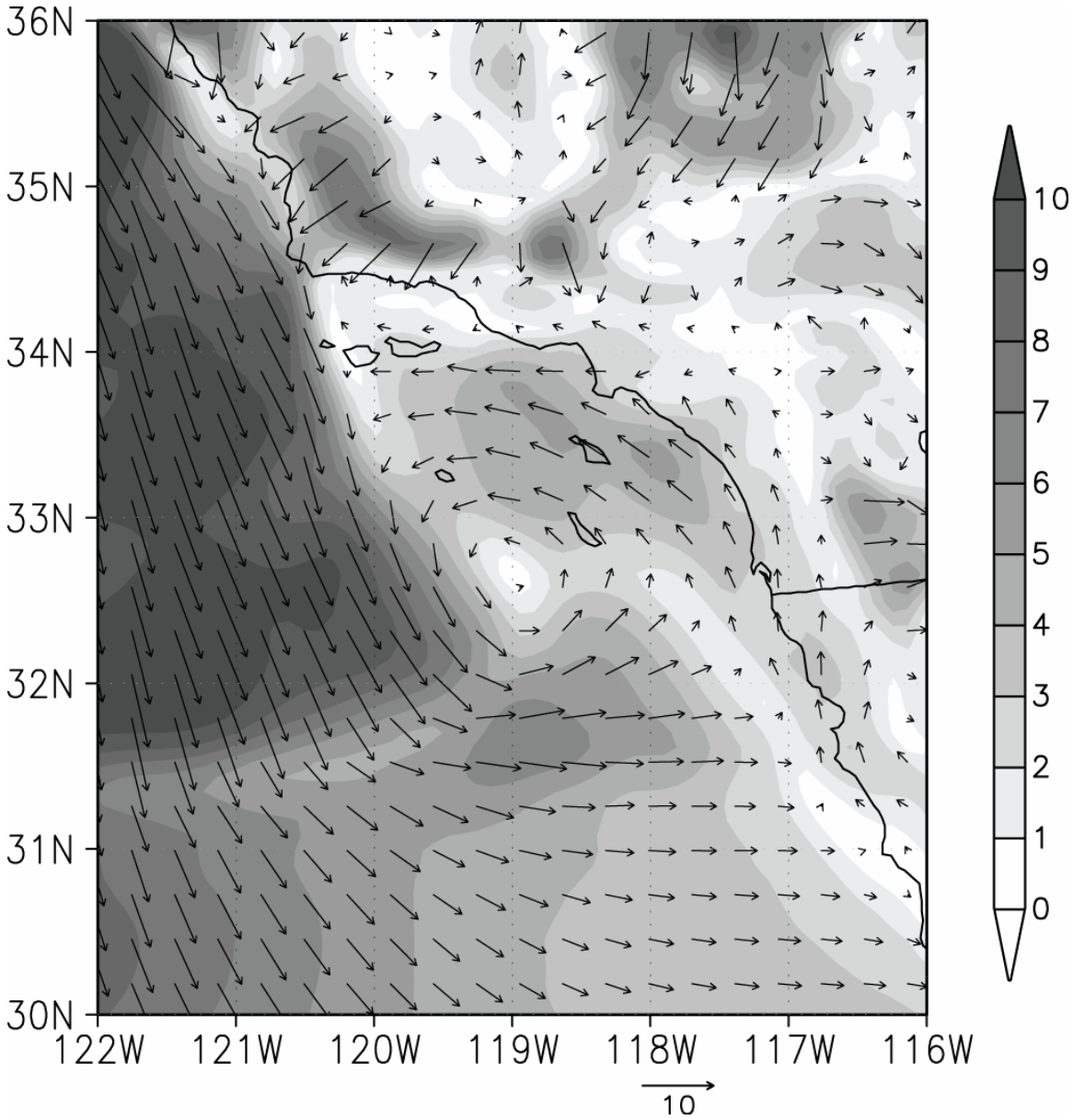

Figure 5. An example of the Catalina Eddy as it appeared in the CaRD10 at 1500UTC, May 22, 1984. Shades and arrows indicate winds at 10m above surface (m s^{-1}).

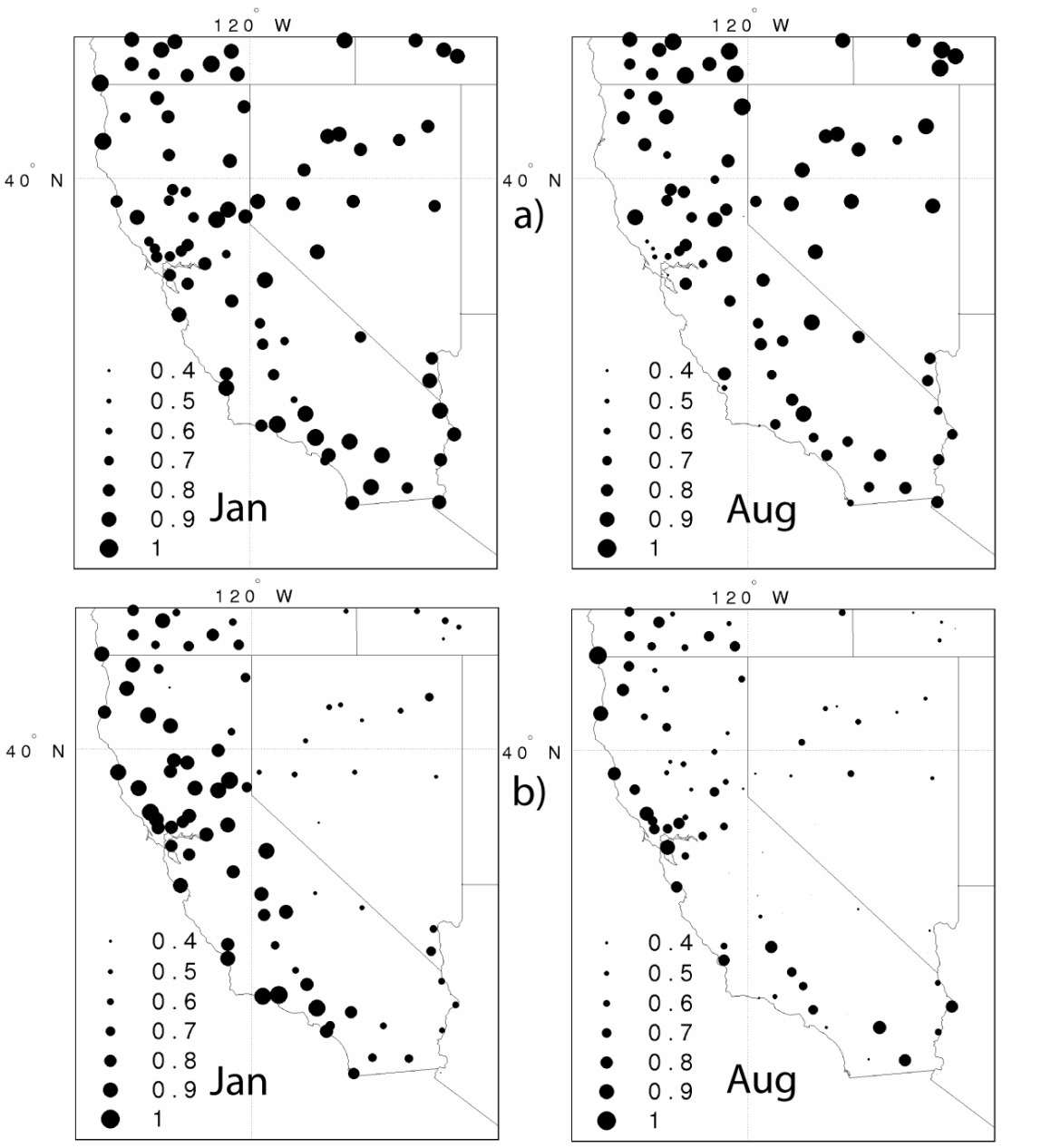

Figure 6. Correlation of monthly average of a) daily mean temperature and b) precipitation with observation for the period 1948-96.

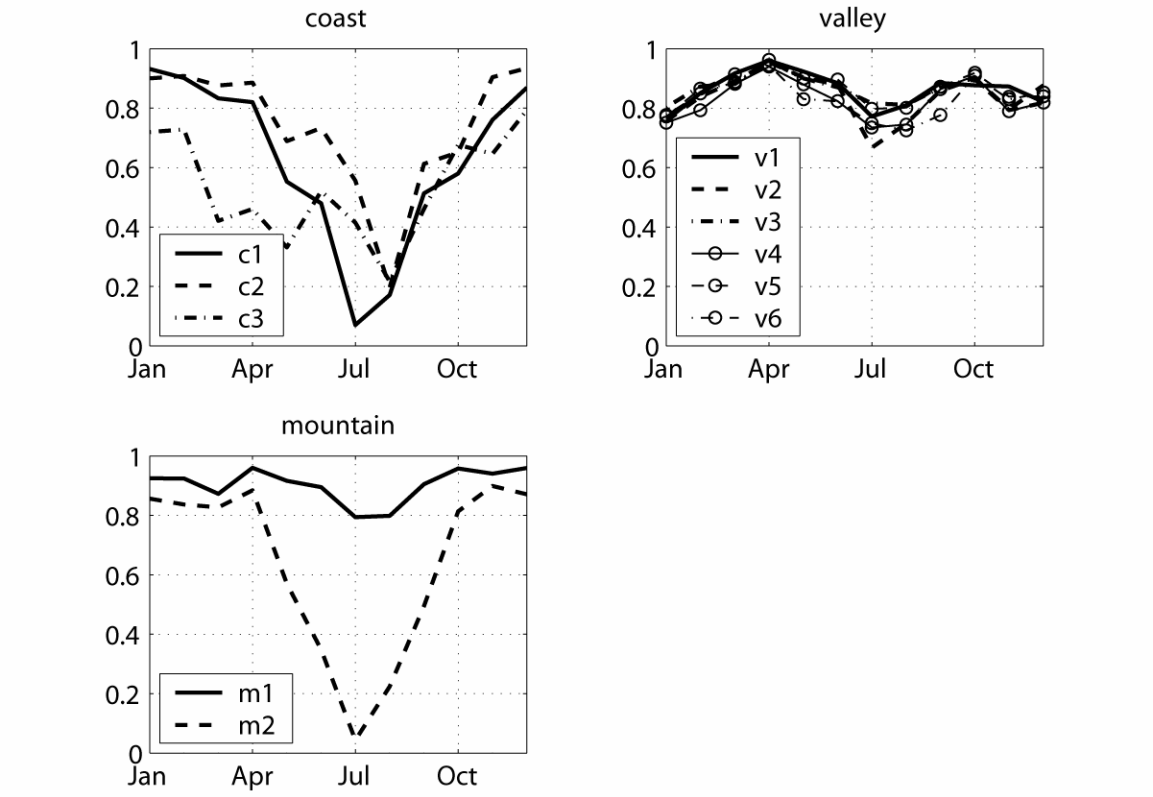

Figure 7. Variation of correlation of monthly mean temperature with observation for the period 1948-96 at coastal (c1 to c3), Central Valley (v1 to v6) and mountain (m1 and m2) stations.

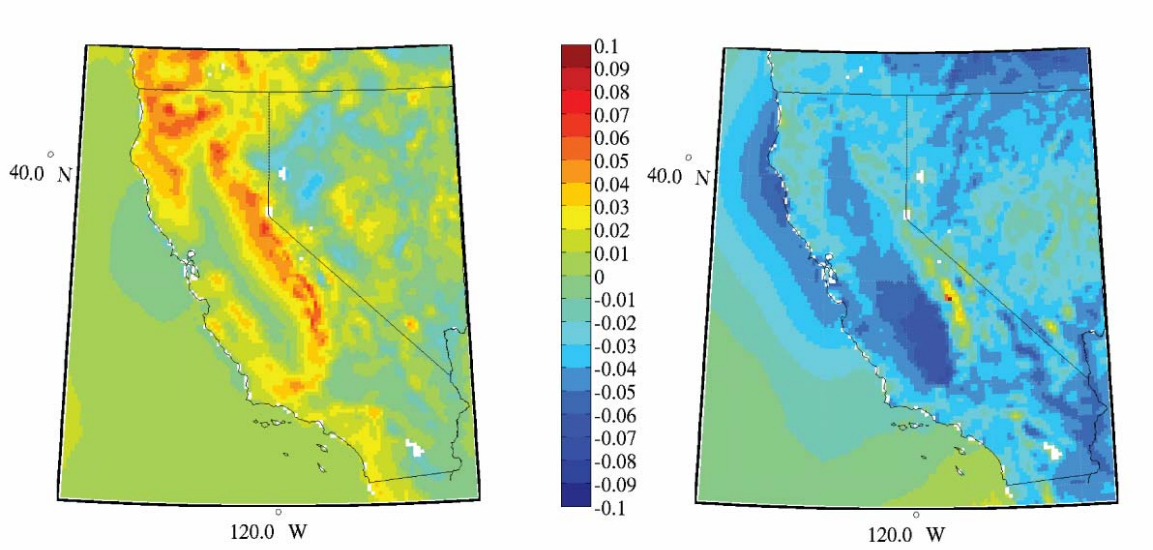

Figure 8. 1950-96 linear trend of 2-meter temperature (K year^{-1}) for January (left) and July (right) in CaRD10.

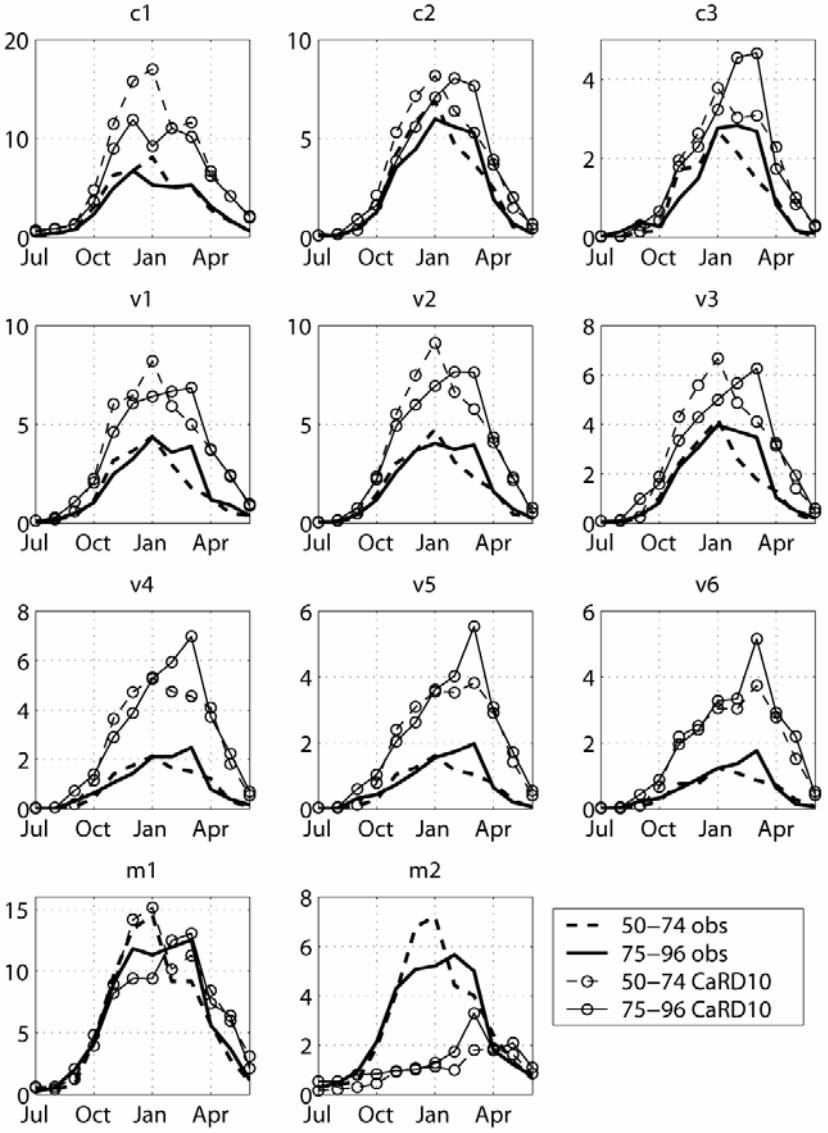

Figure 9. Seasonal variation of monthly averaged precipitation (mm day^{-1})in CaRD10 at 11 selected observation locations. 1950-74 climatology and 1975-96 climatology are plotted separately.

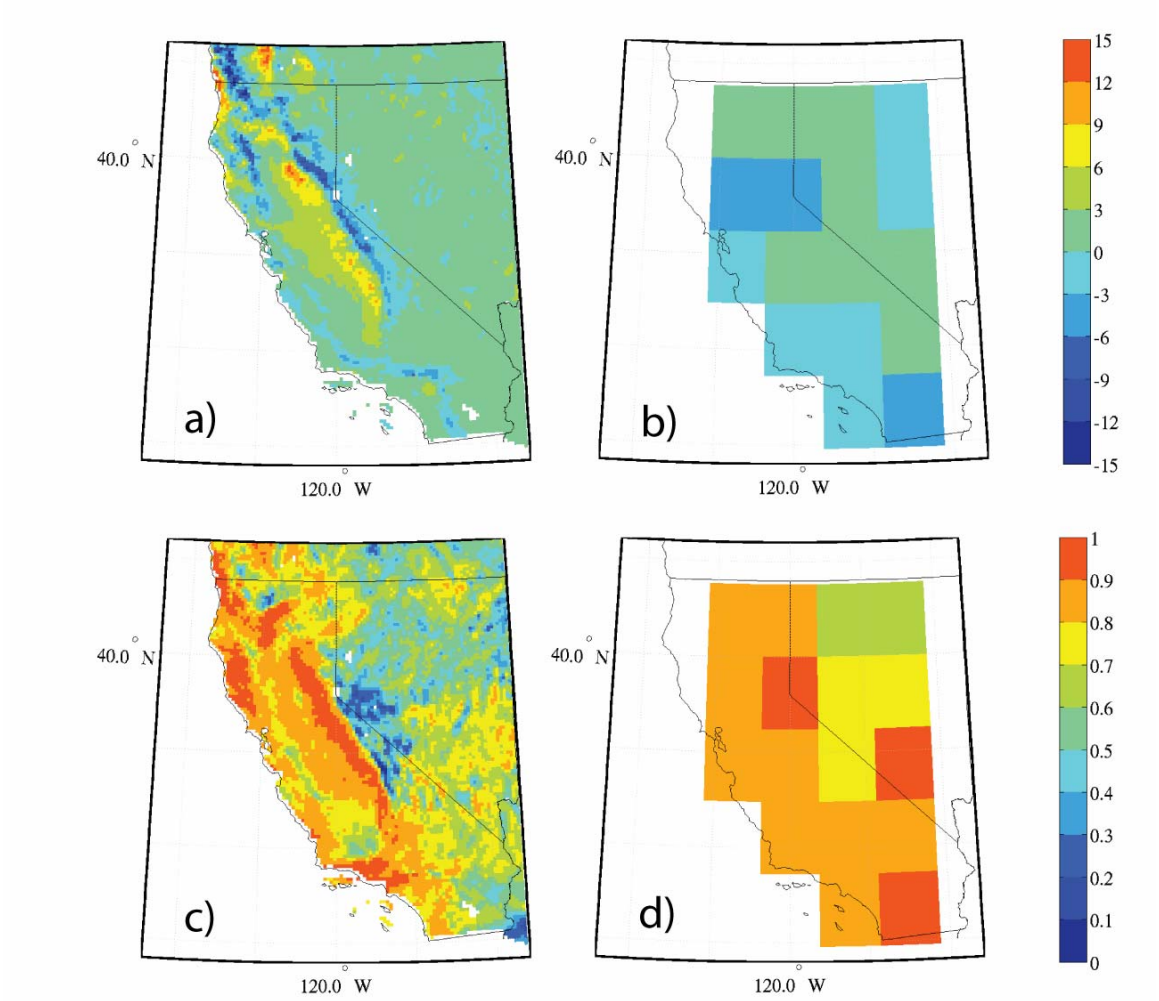

Figure 10. January mean precipitation comparison of CaRD10 and NNR against PRISM analysis for the 1950-97 period. Bias a) in CaRD10 and b) in NNR. Unit mm day^{-1}. Temporal correlations c) in CaRD10 and d) in NNR.

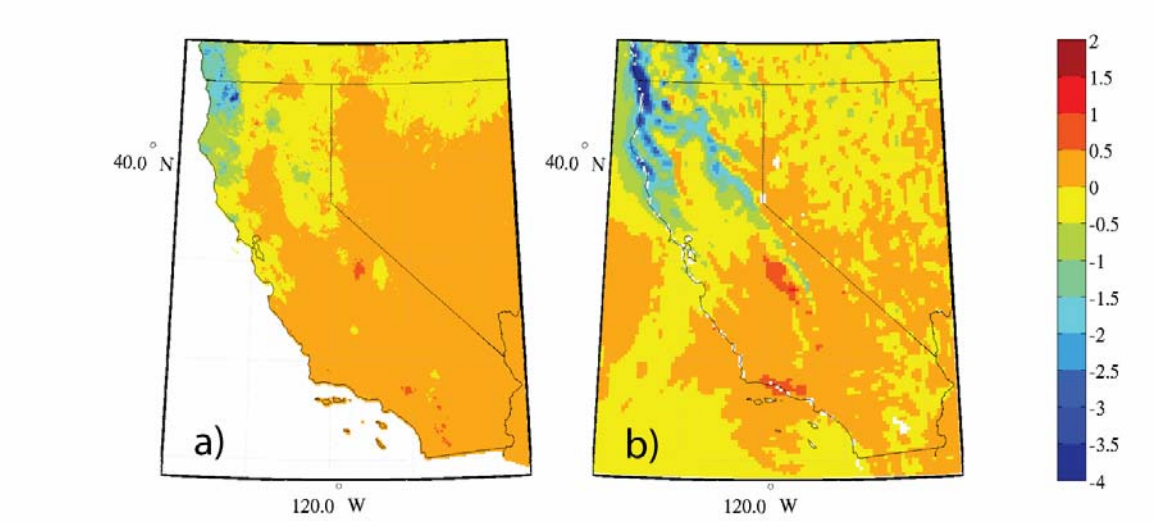

Figure 11. Comparison of the 1950-97 trend in January mean precipitation rate. a) PRISM and b) CaRD10. Unit is in mm day^{-1} $decade^{-1}$.